AAS 21-789

ANALYTIC INITIAL ORBIT DETERMINATION USING SATELLITE STREAKS IN DIGITAL IMAGES

John A. Christian*

Earth orbiting satellites often appear as streaks in images collected by inertially pointed cameras or telescopes. This work presents a novel method of initial orbit determination (IOD) by recognizing that such streaks define a plane tangent to the observed satellite's orbit and passing through the sensor's location. Using results from algebraic projective geometry, an analytic IOD solution may be found by solving for the disk quadric defining the 3D orbit. This solution is exact, recovering the orbit to within machine precision for two-body motion and without measurement noise. Performance in the presence of noisy measurements is also discussed.

INTRODUCTION

Well-known methods exist for determining the orbit of an observed object from a collection of bearing measurements (i.e., so-called angles-only IOD) [1, 2, 3], of position vectors [4], or of velocity vectors [5, 6]. In this work we consider a novel IOD solution for bodies forming streaks in images—a common measurement type encountered within the context of space domain awareness (SDA).

Consider a telescope or camera that produces a digital image. Suppose this optical sensor collects an image with a fixed inertial pointing direction, such that stars appear (nearly) as point sources within the image. Satellites transiting the sensor's field-of-view often appear as streaks in the resulting image. Assuming the data association problem is solved (i.e., we know that the satellite forming a streak in one image is the same satellite forming a streak in another image), we present here a novel IOD algorithm based on algebraic projective geometry. While a brief review of the essentials of algebraic projective geometry are presented here, the reader interested in learning more about this subject is directed to Refs. [7, 8, 9]. The solution developed in this paper is analytic and non-iterative, solving the problem exactly for two-body motion in the absence of measurement noise.

GEOMETRIC PRELIMINARIES

Classical Two-Body Motion

Consider the scenario of a small body (e.g., spacecraft) having a position $\boldsymbol{r}$ relative to a large central body (e.g., Earth). Supposing the central body has a spherically symmetric mass distribution and ignoring all forces other than the gravitational attraction of the central body, we arrive at the classical two-body equations-of-motion,

$$\ddot{\boldsymbol{r}} = -\frac{\mu}{\|\boldsymbol{r}\|^3}\boldsymbol{r} \tag{1}$$

where μ is the central body's gravitational parameter. The solution to Eq. (1) is a conic section and is described by the trajectory equation

$$r = \frac{h^2/\mu}{1 + e\cos\theta} \tag{2}$$

*Associate Professor, Guggenheim School of Aerospace Engineering, Georgia Institute of Technology, Atlanta, GA 30332.

where $r = \|\boldsymbol{r}\|$, $h = \|\boldsymbol{h}\|$ is the magnitude of the specific angular momentum, e is the orbit eccentricity, and θ is the true anomaly. In the discussion that follows we will focus on closed (circular or elliptical) orbits, having $0 \leq e < 1$.

The representation for the orbit conic in Eq. (2) describes the conic locus as expressed in the perifocal frame. Describing the full 3D orbit requires we also capture the orientation of the perifocal frame, which is accomplished using the set of orthonormal basis vectors $\{\boldsymbol{p}, \boldsymbol{q}, \boldsymbol{w}\}$. Here, $\boldsymbol{p}$ is the unit vector in the direction of periapsis, $\boldsymbol{w}$ is the unit vector in the direction of the orbit angular momentum, and $\boldsymbol{q}$ completes the right-handed system.

We note that the classical expression of Eq. 2 is written in polar coordinates, which is not the most convenient representation of a conic section for projective geometry. Thus, we suggest an alternative representation of a two-body orbit that significantly simplifies the mathematics of geometric localization.

The Disk Quadric

The present study is interested in orbit determination with optical systems (e.g., cameras, telescopes). Thus, since the measurements are governed by projective geometry, it is often more convenient to operate in projective space $\mathbb{P}^n$ than in Cartesian space $\mathbb{R}^n$.

A 3D conic (e.g., an orbit) represents a degenerate quadric surface. The locus of points along this 3D conic are most often defined as a conic section, specifically the intersection of a quadric cone (another degenerate quadric surface) and a plane (yet another degenerate quadric surface). Like the trajectory equation in Eq. (2) in conjunction with the perifocal basis $\{\boldsymbol{p}, \boldsymbol{q}, \boldsymbol{w}\}$, this is a mathematically cumbersome way to work with 3D conics when dealing with projective geometry.

A more natural way to represent a 3D Keplerian orbit is with the quadric envelope for a 3D conic—usually referred to as the *disk quadric* [7, 9]. The disk quadric is described by a symmetric 4×4 matrix $\boldsymbol{Q}^*$ of rank three and arbitrary scale that defines all planes $\boldsymbol{\pi}$ that are tangent to the 3D conic. The duality of points and planes in $\mathbb{P}^3$ shows us that

$$\boldsymbol{\pi}^T \boldsymbol{Q}^* \boldsymbol{\pi} = 0 \tag{3}$$

where $\boldsymbol{\pi}$ is a 4×1 vector in $\mathbb{P}^3$ describing a plane tangent to the orbit.

It is straightforward to compute $\boldsymbol{Q}^*$ for an elliptical orbit in terms of the perifocal basis vectors and classical orbital elements

$$\boldsymbol{Q}^* \propto \begin{bmatrix} \boldsymbol{p}\boldsymbol{p}^T + \boldsymbol{q}\boldsymbol{q}^T & (c/b^2)\boldsymbol{p} \\ (c/b^2)\boldsymbol{p}^T & -1/b^2 \end{bmatrix} \tag{4}$$

where $c = ea$ is the distance of the focus form the ellipse center, $b = a\sqrt{1-e^2}$ is the ellipse semi-minor axis, and a is the ellipse semi-major axis. The proportional relationship in Eq. (4) captures the scale ambiguity of $\boldsymbol{Q}^*$. Letting $\alpha = c/b^2$ and $\beta = 1/b$, this is the same as

$$\boldsymbol{Q}^* \propto \begin{bmatrix} \boldsymbol{I} - \boldsymbol{w}\boldsymbol{w}^T & (c/b^2)\boldsymbol{p} \\ (c/b^2)\boldsymbol{p}^T & -1/b^2 \end{bmatrix} = \begin{bmatrix} \boldsymbol{I} - \boldsymbol{w}\boldsymbol{w}^T & \alpha\boldsymbol{p} \\ \alpha\boldsymbol{p}^T & -\beta^2 \end{bmatrix} \tag{5}$$

To see the distinct advantages of this representation of a Keplerian orbit, we first review the geometry of projective cameras.

Projective Cameras and Digital Images

To understand how points (e.g., an unresolved satellite) project into a digital image, we must keep track of a few different coordinate systems. Suppose that a camera (or telescope) located at position $\boldsymbol{s}_I$ observes an orbiting object located at position $\boldsymbol{r}_I$. The subscript I indicates that these quantities are expressed in an inertial frame (e.g., ICRF, TEME). Further suppose that the the camera frame C has an orientation relative to the inertial frame (passive interpretation of a rotation [10]) described by the attitude transformation matrix $\boldsymbol{T}_C^I$, such that

$$\boldsymbol{r}_C = \boldsymbol{T}_C^I \boldsymbol{r}_I \qquad \text{and} \qquad \boldsymbol{s}_C = \boldsymbol{T}_C^I \boldsymbol{s}_I \tag{6}$$

If the observed satellite is unresolved, it will appear as a point in an image. To find the coordinates of this observed point on the focal plane $[x_f, y_f]$ or on the image plane $[x, y]$ we define the ray connecting the camera center to the observed object as a point in $\mathbb{P}^2$ (i.e. a direction in 3D space),

$$\begin{bmatrix} x_f \\ y_f \\ -f \end{bmatrix} \propto \begin{bmatrix} x \\ y \\ 1 \end{bmatrix} \propto \boldsymbol{r}_C - \boldsymbol{s}_C \tag{7}$$

Explicit use of focal plane coordinates is inadvisable. It is generally easier to work entirely in the image plane, as discussed extensively in Ref. [9].

We see that the action of a projective camera viewing a 3D point is a mapping $\mathbb{P}^3 \to \mathbb{P}^2$. To make this mapping explicit, first define the observer and satellite locations as points in $\mathbb{P}^3$ by use of homogeneous coordinates (subscripts omitted since this is true in any frame):

$$\bar{\boldsymbol{r}} = \begin{bmatrix} \boldsymbol{r} \\ 1 \end{bmatrix} \qquad \text{and} \qquad \bar{\boldsymbol{s}} = \begin{bmatrix} \boldsymbol{s} \\ 1 \end{bmatrix} \tag{8}$$

Then the projection onto the image plane is given by

$$\bar{\boldsymbol{x}} = \begin{bmatrix} x \\ y \\ 1 \end{bmatrix} \propto \boldsymbol{P}\bar{\boldsymbol{r}}_I \tag{9}$$

where $\boldsymbol{P}$ is the projection matrix

$$\boldsymbol{P} = \boldsymbol{T}_C^I \begin{bmatrix} \boldsymbol{I} & -\boldsymbol{s}_C \end{bmatrix} \tag{10}$$

The image plane points $[x, y]$ may be converted to pixel coordinates $[u, v]$ in a digital image using the camera calibration matrix. The camera calibration matrix $\boldsymbol{K}$ is given by [9, 11],

$$\boldsymbol{K} = \begin{bmatrix} d_x & \alpha & u_p \\ 0 & d_y & v_p \\ 0 & 0 & 1 \end{bmatrix} \tag{11}$$

and represents a simple affine transformation. An extensive discussion and development is provided in Ref. [9]. Here, d_x is the ratio of focal length to pixel pitch, α is the focal plane array skewness, and $[u_p, v_p]$ are the pixel coordinates of the principal point. The transformation is

$$\bar{\boldsymbol{u}} = \boldsymbol{K}\bar{\boldsymbol{x}} \propto \boldsymbol{K}\boldsymbol{P}\bar{\boldsymbol{r}}_I \qquad \text{or} \qquad \bar{\boldsymbol{x}} = \boldsymbol{K}^{-1}\bar{\boldsymbol{u}} \tag{12}$$

where $\bar{\boldsymbol{u}}^T = [u, v, 1]$. The matrices $\boldsymbol{K}$ and $\boldsymbol{K}^{-1}$ are known for a calibrated camera, which is usually the case for orbit determination applications.

Two-Body Motion with Projective Geometry

We will now develop a few results related to the action of a projective camera on various quantities related to a 3D Keplerian orbit.

Orbit Velocity in 3D using Plücker Matrices The orbit velocity is tangent to the orbit conic and lies in the plane of the orbit. Since imaging using a camera or telescope follows projective geometry, it is instructive to work in projective space $\mathbb{P}^3$ instead of $\mathbb{R}^3$. Therefore, we define the 3D line on which the velocity vector lies using a Plücker matrix.

The most straightforward way to form a Plücker matrix is as the join of two points $\{\boldsymbol{a}, \boldsymbol{b}\} \in \mathbb{R}^3$. We express these as points in $\mathbb{P}^3$ as

$$\bar{\boldsymbol{a}} \propto \begin{bmatrix} \boldsymbol{a} \\ 1 \end{bmatrix} \qquad \bar{\boldsymbol{b}} \propto \begin{bmatrix} \boldsymbol{b} \\ 1 \end{bmatrix} \tag{13}$$

such that the Plücker matrix is a 4×4 skew-symmetric matrix of rank two

$$\boldsymbol{L} \propto \bar{\boldsymbol{a}}\bar{\boldsymbol{b}}^T - \bar{\boldsymbol{b}}\bar{\boldsymbol{a}}^T \tag{14}$$

Therefore, we can construct the line long which the velocity vector lies by defining the points $\bar{\boldsymbol{a}}$ and $\bar{\boldsymbol{b}}$ as

$$\bar{\boldsymbol{a}}_I \propto \begin{bmatrix} \boldsymbol{r}_I \\ 1 \end{bmatrix} \qquad \bar{\boldsymbol{b}}_I \propto \begin{bmatrix} \boldsymbol{r}_I + \alpha \boldsymbol{v}_I \\ 1 \end{bmatrix} \tag{15}$$

where $\alpha \neq 0$ is an arbitrary scale factor. Substitution into Eq. (14) yields the 4×4 skew-symmetric matrix

$$\boldsymbol{L}_I \propto \begin{bmatrix} [(\boldsymbol{v}_I \times \boldsymbol{r}_I)\times] & -\boldsymbol{v}_I \\ \boldsymbol{v}_I^T & 0 \end{bmatrix} \tag{16}$$

Note that the arbitrary scale factor α does not appear in the result.

Now, if $\boldsymbol{L}_I^*$ is the dual of the Plücker matrix [8], then we may compute the 3D plane formed by the join of the 3D line $\boldsymbol{L}_I$ and a point $\bar{\boldsymbol{s}}_I \in \mathbb{P}^3$ as

$$\boldsymbol{\pi}_I \propto \boldsymbol{L}_I^* \bar{\boldsymbol{s}}_I \tag{17}$$

Therefore, if $\boldsymbol{L}_I$ is the 3D line containing the velocity vector [e.g., computed via Eq. (16)] then $\boldsymbol{\pi}_I$ is a plane tangent to the orbit ellipse that also passes thorough the 3D point $\bar{\boldsymbol{s}}_I$. It follows that $\boldsymbol{\pi}_I$ belongs to the quadric envelope described by $\boldsymbol{Q}^*$,

$$\boldsymbol{\pi}_I = \boldsymbol{L}_I^* \bar{\boldsymbol{s}}_I \in \{\boldsymbol{\pi} | \boldsymbol{\pi}^T \boldsymbol{Q}^* \boldsymbol{\pi} = 0\} \tag{18}$$

The projection of the 3D line $\boldsymbol{L}_I$ in an image is the 2D line $\boldsymbol{\ell}$ formed by the intersection of the plane $\boldsymbol{\pi}_I$ and the image plane. The location and orientation of the image plane is governed by the projection matrix $\boldsymbol{P}$ from Eq. (10) and is converted to pixel coordinates using the camera calibration matrix $\boldsymbol{K}$ from Eq. (11). The 2D line $\boldsymbol{\ell}$ in the image is computed directly as

$$[\boldsymbol{\ell}\times] \propto \boldsymbol{K}\boldsymbol{P}\boldsymbol{L}_I\boldsymbol{P}^T\boldsymbol{K}^T \tag{19}$$

where $\boldsymbol{\ell}$ is in units of pixels. An image point $\bar{\boldsymbol{u}}$ lies on this line when

$$\bar{\boldsymbol{u}}^T \boldsymbol{\ell} = 0 \tag{20}$$

Projection of a Keplerian Orbit Suppose we have an orbit described by the disk quadric $\boldsymbol{Q}^*$ from Eq. (4). The projection of the disk quadric into an image is a conic. We may analytically compute this pojection to find the conic envelope $\boldsymbol{C}^*$ in the digital image as

$$\boldsymbol{C}^* \propto \boldsymbol{K}\boldsymbol{P}\boldsymbol{Q}^*\boldsymbol{P}^T\boldsymbol{K}^T \tag{21}$$

The conic envelope defines the set of lines $\boldsymbol{\ell}$ tangent to the conic. From the duality of points and lines in $\mathbb{P}^2$, we know that

$$\boldsymbol{\ell}^T \boldsymbol{C}^* \boldsymbol{\ell} = 0 \tag{22}$$

Clearly, the line $\boldsymbol{\ell}$ defined here is the same as the line $\boldsymbol{\ell}$ computed in Eq. (19). Moreover, if the 2D image point $\bar{\boldsymbol{u}}$ is on an image conic and $\boldsymbol{\ell}$ is the tangent line at that point, then

$$\bar{\boldsymbol{u}} \propto \boldsymbol{C}^* \boldsymbol{\ell} \tag{23}$$

INITIAL ORBIT DETERMINATION FROM STREAK OBSERVATIONS

Consider the case where the observer is stationary (or the spacecraft is moving much faster than the observer) or where the camera/telescope is pointed nearly along the observer's own veloicty vector. In such situations, the streak formed by a spacecraft in a digital image corresponds directly to the line formed by the projection of the velocity vector. Using the results introduced above, this allows for the direct recovery of the disk quadric $\boldsymbol{Q}^*$ from streak observations and, hence, a direct recovery of the observed satellite's orbit. The result is a novel initial orbit determination (IOD) routine for streak observations.

Streak Localization in Digital Images

The first task is to localize the streak within a digital image. We do this with subpixel accuracy using the isolated streak localization procedure presented in Ref. [12]. With points belonging to the streak identified in pixel coordinates, we may fit a line to the streak points—we find this to be an excellent approximation for short exposure times.

Therefore, let the m points belonging to the streak be given by $\{\bar{\boldsymbol{u}}_i\}_{i=1}^m$, where $\bar{\boldsymbol{u}}_i^T = [u_i, v_i, 1]$ is in homogeneous coordinates. Recall that an image point $\bar{\boldsymbol{u}}_i$ lies on the line $\boldsymbol{\ell}$ when the following constraint is satisfied:

$$\bar{\boldsymbol{u}}_i^T \boldsymbol{\ell} = 0 \tag{24}$$

where $\boldsymbol{\ell}$ is a 3×1 vector of arbitrary scale. Thus, given a set of m points belonging to a straight-line streak, we may solve for $\boldsymbol{\ell}$ by solving the linear system

$$\begin{bmatrix} \bar{\boldsymbol{u}}_1^T \\ \bar{\boldsymbol{u}}_2^T \\ \vdots \\ \bar{\boldsymbol{u}}_m^T \end{bmatrix} \boldsymbol{\ell} = \mathbf{0}_{m\times 1} \tag{25}$$

where it is clear that $\boldsymbol{\ell}$ has arbitrary scale. This is a null space problem with an easy solution found via the singular value decomposition (SVD).

Unconstrained IOD from Streaks

Suppose we have n images containing streak observations of the same satellite. For each image we have the observed line $\boldsymbol{\ell}_j$, and observed streak midpoint $\bar{\boldsymbol{u}}_j$, the known projection matrix $\boldsymbol{P}_j$, and the known camera calibration matrix $\boldsymbol{K}_j$.

Begin by considering just the jth image. Recalling Eq. (23), we can remove the unknown proportionality by taking the cross-product with the known streak midpoint $\bar{\boldsymbol{u}}_j$,

$$[\bar{\boldsymbol{u}}_j\times]\,\bar{\boldsymbol{u}}_j = [\bar{\boldsymbol{u}}_j\times]\,\boldsymbol{C}_j^*\boldsymbol{\ell}_j = \mathbf{0}_{3\times 1} \tag{26}$$

where $\boldsymbol{C}_j^*$ describes the apparent conic envelope in the jth image. Now, substituting from Eq. (21)

$$[\bar{\boldsymbol{u}}_j\times]\,\boldsymbol{C}_j^*\boldsymbol{\ell}_j = [\bar{\boldsymbol{u}})j\times]\,\boldsymbol{K}_j\boldsymbol{P}_j\boldsymbol{Q}^*\boldsymbol{P}_j^T\boldsymbol{K}_j^T\boldsymbol{\ell}_j = \mathbf{0}_{3\times 1} \tag{27}$$

where we observe that the only unknown is the symmetric matrix $\boldsymbol{Q}^*$ and that our equation is linear in this unknown. We can rearrange this expression to better isolate the unknowns as

$$[\bar{\boldsymbol{u}}_j\times]\left(\boldsymbol{\ell}_j^T\boldsymbol{K}_j\boldsymbol{P}_j \otimes \boldsymbol{K}_j\boldsymbol{P}_j\right)\mathrm{vec}(\boldsymbol{Q}^*) = \mathbf{0}_{3\times 1} \tag{28}$$

where $\otimes$ is the Kronecker product and $\mathrm{vec}(\cdot)$ is the vectorization operator. Recognizing that $\boldsymbol{Q}^*$ is symmetric we may define the 16×10 duplication matrix $\boldsymbol{D}$ such that

$$\mathrm{vec}(\boldsymbol{Q}^*) = \boldsymbol{D}\boldsymbol{\xi} \tag{29}$$

where $\boldsymbol{\xi}$ is a 10×1 vector of the unique entries in $\boldsymbol{Q}^*$. Therefore, we have

$$[\bar{\boldsymbol{u}}_j\times]\left(\boldsymbol{\ell}_j^T\boldsymbol{K}_j\boldsymbol{P}_j \otimes \boldsymbol{K}_j\boldsymbol{P}_j\right)\boldsymbol{D}\boldsymbol{\xi} = \mathbf{0}_{3\times 1} \tag{30}$$

where the only unknown is $\boldsymbol{\xi}$.

If we now collect this result for all n images, each containing a streak formed by the same satellite, we may construct a linear system

$$\begin{bmatrix} [\bar{\boldsymbol{u}}_1\times]\left(\boldsymbol{\ell}_1^T\boldsymbol{K}_1\boldsymbol{P}_1\otimes\boldsymbol{K}_1\boldsymbol{P}_1\right) \\ [\bar{\boldsymbol{u}}_2\times]\left(\boldsymbol{\ell}_2^T\boldsymbol{K}_2\boldsymbol{P}_2\otimes\boldsymbol{K}_2\boldsymbol{P}_2\right) \\ \vdots \\ [\bar{\boldsymbol{u}}_n\times]\left(\boldsymbol{\ell}_n^T\boldsymbol{K}_n\boldsymbol{P}_n\otimes\boldsymbol{K}_n\boldsymbol{P}_n\right) \end{bmatrix} \boldsymbol{D}\boldsymbol{\xi} = \boldsymbol{0}_{3n\times 1} \tag{31}$$

which requires $n \geq 5$ for a solution. It is possible to solve directly for $\boldsymbol{\xi}$ (and, thus, $\boldsymbol{Q}^*$) in the least squares sense using a SVD.

We note that the estimate of $\boldsymbol{Q}^*$ found in this way is not constrained to have the specific structure of Eq. (4). Applying such constraints reduces the number of required observations, but produces a non-convex quadratically constrained quadratic programming (QCQP) problem. We are presently working on various methods for solving this problem [e.g., Shor relaxation [13, 14]].

The task of recovering the standard conic parameters (e.g., semi-major axis, eccentricity, inclination) is straightforward once $\boldsymbol{Q}^*$ is known. Recovering $\boldsymbol{p}$, $\boldsymbol{q}$, c, and b [see Eq. (4)] is simple if we always scale our solution for $\boldsymbol{Q}^*$ such that $Q^*_{11} + Q^*_{22} + Q^*_{33} = 2$. These can be converted into the classical orbital elements using whatever textbook relations the analyst prefers.

NUMERICAL EXAMPLE

As an illustration, we will consider IOD using observations of a low-Earth orbit (LEO) satellite as seen from three separate ground stations. We consider a LEO orbit with a semi-major axis of $a = 7420$ km, an eccentricity of $e = 0.1$, and an inclination of $i = 60$ deg. The orbit is observed from ground stations located at latitudes of 30 deg, 45 deg, and -35 deg. If three streak observations are made during each pass, the observation geometry is similar to that shown in Fig. 1.

In the absence of measurement error or observer motion, the orbit is recovered to machine precision. Now, suppose the optical observations have a bearing error of 1 arcmin (1/60 deg) and an error in image streak orientation of 0.1 deg. A 5,000-run Monte Carlo analysis was performed to assess the orbit determination performance in such a scenario, both with and without observer motion. The orbit determination performance is summarized in Table 1.

The results of Table 1 make intuitive sense. First, we note that errors in the direction of $\boldsymbol{w}$ are significantly smaller than errors in the direction of $\boldsymbol{p}$. That is, the orientation of the orbit plane is more observable that the direction to periapsis. This is a result of the measurements being tangent planes with the observer always being close to the orbit plane. It is also an artifact of the relatively low eccentricity.

We also observe that including the observer motion (which always is present in practice) reduces performance. This is because the streak is formed by the relative velocity between the observer and the satellite, and not just the satellite's velocity alone. Hence, the plane formed by the streak and observer location is not perfectly tangent to the orbit. Methods for mitigating this are a topic of ongoing research.

Table 1. Orbit determination performance (1σ) from a 5,000-run Monte Carlo simulation.

Orbit Parameter	Stationary Observer	Moving Observer
Direction of $\boldsymbol{p}$	0.6753 deg	7.909 deg
Direction of $\boldsymbol{w}$	0.0997 deg	1.216 deg
Semi-major axis, a	15.73 km	217.66 km
Eccentricity, e	0.0011	0.0168

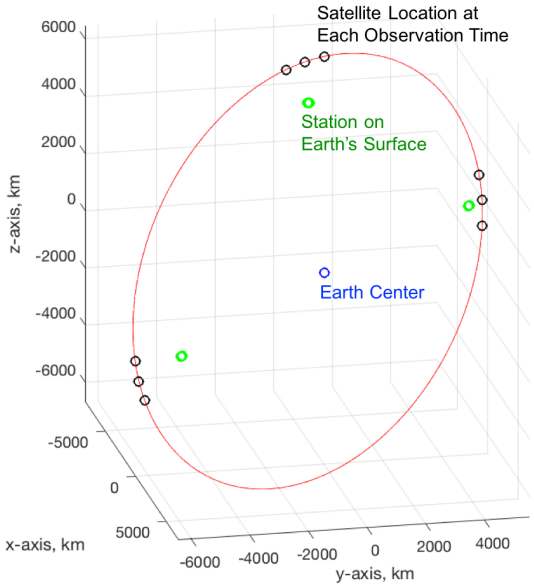

Figure 1. Illustration of 3D orbit (red) as viewed by stations on the Earth's surface. A total of nine observations are made, with the observer location shown in green and the spacecraft location shown by black dots.

CONCLUSIONS

This work provides some initial steps in the application of algebraic projective geometry to the problem of initial orbit determination (IOD) for an object obeying Keplerian motion. A number of useful relations are developed for the disk quadric describing the 3D orbit conic and for the Plüker matrix describing the line on which orbit velocity vectors lie. Analytic relations exist for projecting these constructs onto an image. The utility of this is illustrated with a novel streak-based IOD algorithm.

REFERENCES

[1] S. Laplace, "Mémoire sur la Détermination des Orbites des Comètes," *Mémoires de Mathématique et de Physique*, 1780, pp. 13–72.

[2] C. F. Gauss, *Theoria Motus Corporum Coelestium in Sectionibus Conicis Solem Ambientum*. Hamburg: F. Perthes and I.H. Besser, 1809.

[3] P. R. Escobal, *Methods of Orbit Determination*. Malabar, FL: Robert E. Krieger Publishing Company, 2nd ed., 1976.

[4] J. Gibbs, "On the Determination of Elliptic Orbits from Three Complete Observations," *Memoirs of the National Academy of Sciences*, Vol. 4, No. 8, 1889, pp. 79–104.

[5] C. L. Hollenberg and J. A. Christian, "Geometric Solutions for Problems in Velocity-Based Orbit Determination," *Journal of the Astronautical Sciences*, Vol. 67, 2019, pp. 188–224, 10.1007/s40295-019-00170-7.

[6] J. A. Christian, "StarNAV: Autonomous Optical Navigation of a Spacecraft by the Relativistic Perturbation of Starlight," *Sensors*, Vol. 19, No. 4064, 2019, 10.3390/s19194064.

[7] J. G. Semple and G. T. Kneebone, *Algebraic Projective Geometry*. Oxford, UK: Oxford University Press, 1952.

[8] R. Hartley and A. Zisserman, *Multiple View Geometry, 2nd Ed.* Cambridge, UK: Cambridge University Press, 2003.

[9] J. A. Christian, "A Tutorial on Horizon-Based Optical Navigation and Attitude Determination with Space Imaging Systems," *IEEE Access*, 2021, pp. 19819–19853, 10.1109/ACCESS.2021.3051914.

[10] R. Zanetti, "Rotations, Transformations, Left Quaternions, Right Quaternions?," *The Journal of the Astronautical Sciences*, Vol. 66, 2019, pp. 361–381, 10.1007/s40295-018-00151-2.

[11] J. A. Christian, L. Benhacine, J. Hikes, and C. D'Souza, "Geometric Calibration of the Orion Optical Navigation Camera using Star Field Images," *The Journal of the Astronautical Sciences*, Vol. 63, No. 4, 2016, pp. 335–353, 10.1007/s40295-016-0091-3.

[12] D. T. Renshaw and J. A. Christian, "Subpixel Localization of Isolated Edges and Streaks in Digital Images," *Journal of Imaging*, Vol. 6, No. 33, 2020, 10.3390/jimaging6050033.

[13] N. Z. Shor, "Quadratic optimization problems," *Soviet Journal of Circuits and Systems Science*, Vol. 25, No. 6, 1987, pp. 1–11.

[14] L. Vandenberghe and S. Boyd, "Semidefinite Programming," *SIAM Review*, Vol. 38, No. 1, 1996, pp. 49–95.